Monodisperse FePt Nanoparticles and Ferromagnetic FePt Nanocrystal Superlattices

Shouheng Sun,[1]* C. B. Murray,[1] Dieter Weller,[2] Liesl Folks,[2] Andreas Moser[2]

Synthesis of monodisperse iron-platinum (FePt) nanoparticles by reduction of platinum acetylacetonate and decomposition of iron pentacarbonyl in the presence of oleic acid and oleyl amine stabilizers is reported. The FePt particle composition is readily controlled, and the size is tunable from 3- to 10-nanometer diameter with a standard deviation of less than 5%. These nanoparticles self-assemble into three-dimensional superlattices. Thermal annealing converts the internal particle structure from a chemically disordered face-centered cubic phase to the chemically ordered face-centered tetragonal phase and transforms the nanoparticle superlattices into ferromagnetic nanocrystal assemblies. These assemblies are chemically and mechanically robust and can support high-density magnetization reversal transitions.

The synthesis of nanoparticles with controlled size and composition is of fundamental and technological interest. The effort to understand the physics of ever smaller structures has been paralleled by attempts to exploit their beneficial properties. The increased surface area and tailored surface chemistry of metal nanoparticles have long been used to optimize the activity and specificity of catalysts (*1*). Semiconductor nanocrystals show size-tunable optical properties and have been integrated into exploratory optical and electronic devices (*2*, *3*). Engineering the interparticle spacing of metal particle arrays has revealed evidence of tunable metal-insulator transitions (*4*). Small metal particle arrays have been used to build single-electron devices (*5*, *6*). Progress in ultrahigh-density magnetic recording is due in part to the development of metal thin film media with smaller particles, tighter size distributions, and optimized compositions (*7*, *8*). Recently, the study of magnetization processes on nanometer length scales has intensified (*9*, *10*).

We report on the synthesis of monodisperse FePt nanoparticles with controlled size and composition and the fabrication of ferromagnetic FePt nanocrystal superlattice assemblies with tunable interparticle spacings. FePt alloys are an important class of materials in permanent magnetic applications because of their large uniaxial magnetocrystalline anisotropy [$K_u \cong 7 \times 10^6$ J/m^3 (*11*)] and good chemical stability. As the magnetic stability of individual particles scales with the anisotropy constant, K_u, and the particle volume, V, small FePt particles may be suitable for future ultrahigh-density magnetic recording media applications (*12*). Until now, the synthesis of FePt particle thin films has mainly relied on vacuum deposition techniques (*13*–*15*). Postdeposition annealing has proven essential to transform the as-deposited chemically disordered face-centered cubic (fcc) structure into the chemically ordered face-centered tetragonal (fct) phase, which has high K_u. Random nucleation in the initial stages of growth, however, typically results in broad distributions of particle sizes, which may be further aggravated by agglomeration during annealing. Solution phase chemical synthesis, in contrast, has been successfully used to prepare monodisperse metal particles (*16*–*19*). However, synthetic procedures have not yet been developed to prepare monodisperse hard magnetic FePt nanoparticles.

To prepare FePt nanoparticles, we used a combination of oleic acid and oleyl amine to stabilize the monodisperse FePt colloids and prevent oxidation. The synthesis is based on the reduction of $Pt(acac)_2$ (acac = acetylacetonate, $CH_3COCHCOCH_3$) by a diol and the decomposition of $Fe(CO)_5$ in high-temperature solutions. The use of diol or polyalcohol (for example, ethylene glycol or glycerol) to reduce metal salts to metal particles is referred to as the "polyol process" (*20*). We modified this procedure by using a long-chain 1,2-hexadecanediol to reduce the $Pt(acac)_2$ to Pt metal. Thermal decomposition of $Fe(CO)_5$ has been used to produce Fe particles (*17*). Both chemical reactions were initiated together in the presence of oleic acid and oleyl amine, providing a convenient route to monodisperse FePt nanoparticles (*21*).

The size and composition of these FePt nanoparticles can be readily controlled. Their composition is adjusted by controlling the molar ratio of iron carbonyl to the platinum salt. For example, with dioctylether as solvent, a 3:2 molar ratio of $Fe(CO)_5$ to $Pt(acac)_2$ gave $Fe_{48}Pt_{52}$ particles, a 2:1 molar ratio yielded $Fe_{52}Pt_{48}$, and a 4:1 molar ratio produced $Fe_{70}Pt_{30}$ (*22*). The FePt particle size can be tuned from 3 to 10 nm by first growing 3-nm monodisperse seed particles in situ and then adding more reagents to enlarge the existing seeds to the desired size. These particles are isolated and purified by centrifugation after the addition of a flocculent (for example, ethanol) and can be redispersed in nonpolar solvents in a variety of concentrations (*23*).

When the FePt colloids are spread on a substrate and the carrier solvent is allowed to slowly evaporate, FePt nanoparticle superlattices are produced (*24*). A drop (~0.5 μl) of dilute FePt dispersion (~1 mg/ml) was deposited on a SiO-coated copper grid for transmission electron microscopy (TEM) studies. The results reveal that the particles are monodisperse with $\sigma \leq 5\%$ in diameter and readily self-assemble into three-dimensional (3D) superlattices. A TEM image (Fig. 1A) shows a thin section of a hexagonal close-packed 3D array of 6-nm $Fe_{50}Pt_{50}$ particles with a nearest neighbor spacing of ~4 nm maintained by the oleic acid and oleyl amine capping groups. Room temperature ligand exchange of these long-chain capping groups for shorter $RCOOH/RNH_2$ (R = dodecyl down to hexyl chains) allows the interparticle distance to be adjusted. Ligand exchange with hexanoic acid/hexylamine yields a cubic packed multilayer of 6-nm $Fe_{50}Pt_{50}$ particles with ~1-nm spacings (Fig. 1B). Such a transition from hexagonal to cubic packing has been observed in monodisperse cobalt nanoparticle assemblies (*19*). The symmetry of the observed superlattices is influenced by several experimental parameters including the relative dimensions of the metal core and the organic capping, as well as the annealing history of the sample. The FePt particle assemblies show no obvious aggregation upon annealing at temperatures up to 600°C under static N_2 atmosphere (1 atm). High-resolution scanning electron microscopy (HRSEM) was used to image the annealed FePt particle assembly on a thermally oxidized Si substrate. For a 180-nm-thick, 4-nm $Fe_{52}Pt_{48}$ particle assembly annealed at 560°C for 30 min, the HRSEM images of both surface (Fig. 1C) and cross section (not shown in figure) of the assembly show that the particles are well separated with no agglomeration occurring. Interparticle spacings, however, are reduced from ~4 to ~2 nm, as indicated by TEM, HRSEM, and small angle x-ray scattering experiments. Some coherent strain is observed in the superlattices because of this shrinkage. Rutherford backscattering measurements on these annealed 4-nm $Fe_{52}Pt_{48}$ particle assemblies indicate 40 to 50% (atomic %) carbon content. This shows that annealing at high temperature does not result in the loss of stabilizing ligands; rather, they are converted to a carbonaceous coating

[1]IBM T. J. Watson Research Center, Yorktown Heights, NY 10598, USA. [2]IBM Almaden Research Center, 650 Harry Road, San Jose, CA 95120, USA.

*To whom correspondence should be addressed. E-mail: ssun@us.ibm.com

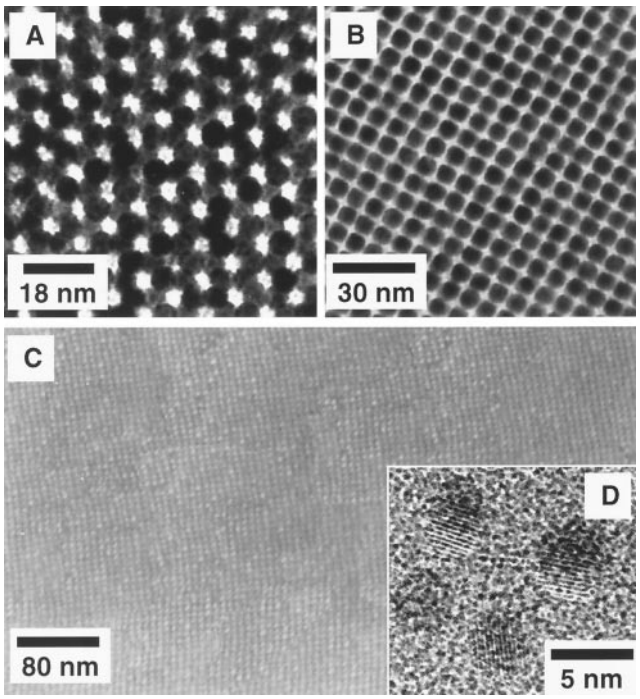

Fig. 1. (**A**) TEM micrograph of a 3D assembly of 6-nm as-synthesized $Fe_{50}Pt_{50}$ particles deposited from a hexane/octane (v/v 1/1) dispersion onto a SiO-coated copper grid. (**B**) TEM micrograph of a 3D assembly of 6-nm $Fe_{50}Pt_{50}$ sample after replacing oleic acid/oleyl amine with hexanoic acid/hexylamine. (**C**) HRSEM image of a ~180-nm-thick, 4-nm $Fe_{52}Pt_{48}$ nanocrystal assembly annealed at 560°C for 30 min under 1 atm of N_2 gas. (**D**) High-resolution TEM image of 4-nm $Fe_{52}Pt_{48}$ nanocrystals annealed at 560°C for 30 min on a SiO-coated copper grid.

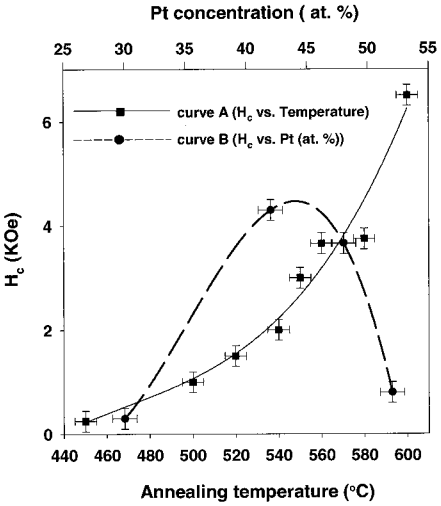

Fig. 3. Curve A shows the in-plane coercivity of a series of ~140-nm-thick, 4-nm $Fe_{52}Pt_{48}$ assemblies as a function of annealing temperature. Each sample is annealed for 30 min under 1 atm of N_2 gas. Curve B indicates the composition-dependent coercivity of ~140-nm-thick FePt assemblies annealed at 560°C for 30 min.

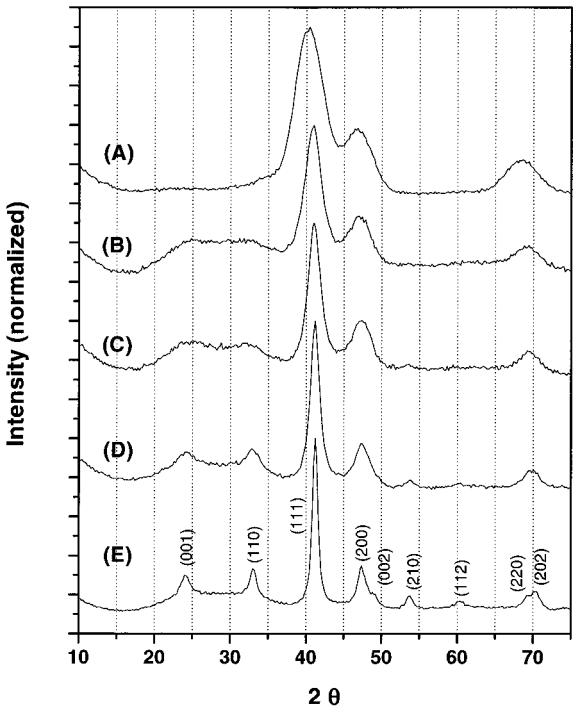

Fig. 2. XRD patterns (**A**) of as-synthesized 4-nm $Fe_{52}Pt_{48}$ particle assemblies and a series of similar assemblies annealed under atmospheric N_2 gas for 30 min at temperatures of (**B**) 450°C, (**C**) 500°C, (**D**) 550°C, and (**E**) 600°C. The indexing is based on tabulated fct FePt reflections (*25*). The diffraction patterns were collected with a Siemens D-500 diffractometer with Cu Kα radiation (wavelength λ = 1.54056 Å).

around each particle. Energy dispersive x-ray spectroscopy measurements carried out during the SEM and scanning TEM imaging of the films confirm that the average nanocrystals are slightly iron-rich and that the carbon is intimately associated with the particles.

Electron diffraction of the as-synthesized $Fe_{52}Pt_{48}$ particles reveals a typical fcc pattern whereas $Fe_{52}Pt_{48}$ particles annealed at 560°C show an fct internal structure. Figure 1D is a high-resolution TEM micrograph of individual 4-nm $Fe_{52}Pt_{48}$ particles annealed at 560°C for 30 min. The particles are single crystals with a lattice spacing of 2.20 Å, characteristic of the (111) planes in the chemically ordered fct FePt phase (*25*). The change of the internal particle crystal structure upon annealing is seen in wide-angle x-ray diffraction (XRD) studies. Figure 2 shows a series of such XRD patterns for ~1-μm-thick $Fe_{52}Pt_{48}$ assemblies as a function of annealing temperature at a constant annealing time of 30 min. As-synthesized particles exhibit the chemically disordered fcc structure (Fig. 2A). Annealing induces the Fe and Pt atoms to rearrange into the long-range chemically ordered fct structure, as indicated by the (111) peak shifts and evolution of the (001) and (110) peaks (Fig. 2, B to E). At annealing temperatures below 500°C, only partial chemical ordering is observed (Fig. 2, B and C). The chemical ordering can be increased by annealing at higher temperatures (Fig. 2, D and E) or by increasing the annealing time (not shown in figure). Diffraction patterns of the samples annealed above 540°C match those of fct FePt (*11*, *25*). Fitting of the XRD line shapes of the sample annealed at 550°C confirms that the particles are individual single crystals with dimensions matching the average particle size of 4 nm (σ = 5% in diameter) determined by statistical analysis of the TEM images. Annealing 4-nm $Fe_{52}Pt_{48}$ particles at higher temperature, for example, ≥600°C, however, results in an increase of the average particle size and a broadening of the size distribution based on TEM and XRD analyses.

Superconducting quantum interference device magnetometry measurements of 4-nm FePt particles show that the as-synthesized particle assemblies are superparamagnetic (coercivity H_c = 0 Oe) at room temperature. The temperature-dependent magnetization was measured in a 10-Oe field between 5 and 400 K with the standard zero–field-cooling and field-cooling procedures (*26*). These studies indicate that superparamagnetic behavior is blocked at 20 to 30 K. This low blocking temperature is consistent with low magnetocrystalline anisotropy of the fcc structure. Annealing converts the particles to the high-anisotropy fct phase and transforms them into room temperature

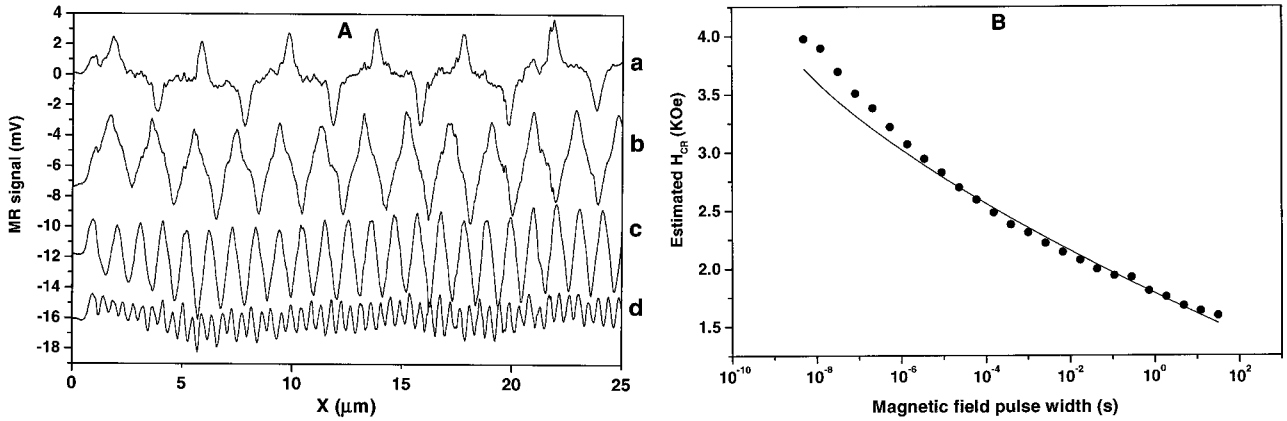

Fig. 4. (**A**) Magneto-resistive (MR) read-back signals from written bit transitions in a 120-nm-thick assembly of 4-nm-diameter $Fe_{48}Pt_{52}$ nanocrystals. The individual line scans reveal magnetization reversal transitions at linear densities of (a) 500, (b) 1040, (c) 2140, and (d) 5000 fc/mm. (**B**) Dynamic coercivity measurements (H_{CR}) of the sample in (A) at 300 K over a range from 5 ns to 65 s. The measured data (●) are fit to a dynamic coercivity law for pulse width $> 10^{-6}$ s (solid curve) (*28*).

nanoscale ferromagnets. The coercivity of these ferromagnetic assemblies is tunable by controlling annealing temperature and time, as well as the Fe:Pt ratio and particle size. Curve A of Fig. 3 shows representative in-plane coercivity data of a series of ~140-nm-thick, 4-nm $Fe_{52}Pt_{48}$ samples as a function of annealing temperature. There is little difference between in-plane and out-of-plane coercivities and hysteresis behavior, indicating random orientation of the easy axes of individual FePt nanocrystals. FePt stoichiometry-dependent coercivity data (curve B of Fig. 3) demonstrate that Fe-rich Fe_xPt_{1-x} ($x \sim 0.52$ to 0.60) nanocrystal assemblies have the largest coercivity, consistent with earlier reports on vacuum-deposited FePt thin films (*12*, *27*).

The annealed FePt nanocrystal assemblies are smooth ferromagnetic films that can support high-density magnetization reversal transitions (bits). A ~120-nm-thick assembly of 4-nm $Fe_{48}Pt_{52}$ nanocrystals with an in-plane coercivity of $H_c = 1800$ Oe was selected for initial recording experiments. Atomic force microscopy studies of this sample indicate a 1-nm root-mean-square variation in height over areas of 3 μm by 3 μm. A static write/read tester was used for the recording experiments (*28*). The read-back sensor voltage signals (Fig. 4A) from written data tracks correspond to linear densities of 500, 1040, 2140, and 5000 flux changes per millimeter (fc/mm) (curves a to d, respectively). These write/read experiments demonstrate that this 4-nm $Fe_{48}Pt_{52}$ ferromagnetic nanocrystal assembly supports magnetization reversal transitions at moderate linear densities that can be read back nondestructively. Much higher recording densities, beyond the highest currently achievable linear densities of ~20,000 fc/mm, can be expected if the thickness of these ferromagnetic assemblies can be reduced to ~4 nm. On the basis of conventional grain size scaling arguments, such media should support recording densities about 10 times larger than the CoCr-based alloy media presently used industry wide (*12*). A critical factor in achieving such a goal is the thermal stability of the magnetic transitions, which can be assessed with a dynamic coercivity method. This method relies on remanent coercivity measurements as a function of the applied magnetic field pulse width (*29*). Figure 4B shows such data, from which the ratio of the energy barrier for magnetization reversal (K_uV) to the thermal energy (k_BT, where k_B is the Boltzmann constant and T is the temperature) is extracted as an inverse slope parameter (*29*). In a simple uniform rotation picture, which is justified for the present small, isolated particles, the inverse slope becomes $\langle K_u \rangle \langle V \rangle / k_BT = 48$. An average anisotropy constant of $\langle K_u \rangle = 5.9 \times 10^6$ J/m^3 can be extracted, assuming spherical 4-nm-diameter particles. These preliminary results raise the expectation that thinner and higher coercivity assemblies will indeed permit drastically reduced bit cell sizes.

The present synthesis provides a simple procedure for the preparation of monodisperse FePt nanoparticles and ferromagnetic FePt nanocrystal superlattice assemblies. The reported control of particle size, composition, crystal structure, and interparticle spacings will enable rigorous testing of current theoretical descriptions of nanometer-scale magnetics. Initial recording studies demonstrate that an assembly of magnetic nanocrystals as small as 4 nm can support stable magnetization reversal transitions (bits) at room temperature. It is expected that optimized ferromagnetic nanocrystal superlattices may contribute to future magnetic recording at areal densities in the terabits per square inch regime.

References and Notes

1. J. S. Bradley, in *Cluster and Colloids*, G. Schmid, Ed. (VCH, New York, 1994), chap. 6.
2. C. B. Murray, C. R. Kagan, M. G. Bawendi, *Science* **270**, 1335 (1995).
3. A. P. Alivisatos, *Science* **271**, 933 (1996).
4. C. P. Collier, R. J. Saykally, J. J. Shiang, S. E. Henrichs, J. R. Heath, *Science* **277**, 1978 (1997).
5. R. P. Andres *et al.*, *Science* **272**, 1323 (1996).
6. D. Davidovic and M. Tinkham, *Appl. Phys. Lett.* **73**, 3959 (1998).
7. T. Yogi *et al.*, *IEEE Trans. Magn.* **26**, 2271 (1990).
8. J. Li *et al.*, *J. Appl. Phys.* **85**, 4286 (1999).
9. S. A. Majetich and Y. Jin, *Science* **284**, 470 (1999).
10. C. H. Back *et al.*, *Science* **285**, 864 (1999).
11. K. Inomata, T. Sawa, S. Hashimoto, *J. Appl. Phys.* **64**, 2537 (1988).
12. D. Weller and A. Moser, *IEEE Trans. Magn.* **35**, 4423 (1999).
13. K. R. Coffey, M. A. Parker, J. K. Howard, *IEEE Trans. Magn.* **31**, 2737 (1995).
14. N. Li and B. M. Lairson, *IEEE Trans. Magn.* **35**, 1077 (1999).
15. R. A. Ristau, K. Barmak, L. H. Lewis, K. R. Coffey, J. K. Howard, *J. Appl. Phys.* **86**, 4527 (1999).
16. G. Schmid, *Chem. Rev.* **92**, 1709 (1992).
17. K. S. Suslick, M. Fang, T. Hyeon, *J. Am. Chem. Soc.* **118**, 11960 (1996).
18. S. Sun and C. B. Murray, *J. Appl. Phys.* **85**, 4325 (1999).
19. ———, H. Doyle, *Mat. Res. Soc. Symp. Proc.* **577**, 385 (1999).
20. F. Fiévet, J. P. Lagier, M. Figlarz, *MRS Bull.* **14**, 29 (1989).
21. One typical synthetic procedure is as follows: under airless condition, platinum acetylacetonate (197 mg, 0.5 mmol), 1,2-hexadecanediol (390 mg, 1.5 mmol), and dioctylether (20 ml) were mixed and heated to 100°C. Oleic acid (0.16 ml, 0.5 mmol), oleyl amine (0.17 ml, 0.5 mmol), and $Fe(CO)_5$ (0.13 ml, 1 mmol) were added, and the mixture was heated to reflux (297°C). The refluxing was continued for 30 min. The heat source was then removed, and the reaction mixture was allowed to cool to room temperature. The inert gas protected system could be opened to ambient environment at this point. The black product was precipitated by adding ethanol (~40 ml) and separated by centrifugation. Yellow-brown supernatant was discarded. The black precipitate was dispersed in hexane (~25 ml) in the presence of oleic acid (~0.05 ml) and oleyl amine (~0.05 ml) and precipitated out by adding ethanol (~20 ml) and centrifuging. The product was dispersed in hexane (~20 ml), centrifuged to remove any unsolved precipitation (almost no precipitation was found at this stage), and precipitated out by adding ethanol (~15 ml) and centrifuging. The materials were redispersed

in hexane and stored under N_2. The total weight of material recovered was 162 mg.
22. The elemental composition of the as-synthesized FePt particle materials was obtained by inductively coupled plasma–atomic emission spectrometry. The samples were precipitated from hexane dispersions by adding ethanol and then drying. The analysis was performed at Galbraith Laboratories (Knoxville, TN).
23. Although the particle dispersion can be handled without inert gas protection, it is advisable to store the hexane dispersion under N_2 for long-term protection.
24. An example is as follows: 0.02 ml of hexane-dispersed FePt nanoparticles (equivalent to ~5 mg/ml) was deposited on a SiO_2/Si substrate (~0.5 cm by 1 cm). The solvent was allowed to evaporate slowly (~5 min) at room temperature. The as-deposited thin film was then transferred into a N_2 glove box (O_2 concentration <2 ppm) and annealed in a Thermolyne 1300 furnace. The temperature was raised to 550°C from room temperature over a period of 13 min and maintained for 30 min. The sample was taken out of the furnace and cooled to room temperature in the N_2 box. Composition and thickness of the FePt nanocrystal assembly were determined by Rutherford backscattering spectrometry. This procedure yielded a ~120-nm-thick FePt nanocrystal assembly.
25. Powder Diffraction File 43-1359 (International Center for Diffraction Data, Newtown Square, PA, 1994).
26. M. Hanson, C. Johansson, M. S. Pedersen, S. Mørup, *J. Phys. Condens. Matter* **7**, 9269 (1995).
27. M. H. Hong, K. Hono, M. Watanabe, *J. Appl. Phys.* **84**, 4403 (1998).
28. A. Moser, D. Weller, M. E. Best, M. F. Doerner, *J. Appl. Phys.* **85**, 5018 (1999).
29. A. Moser, D. Weller, M. F. Doerner, *Appl. Phys. Lett.* **75**, 1604 (1999).
30. We thank J. Bruley and A. Kellock for their help with high-resolution TEM and Rutherford backscattering measurements. D.W. and L.F. gratefully acknowledge support by Advanced Materials Research Institute and the Department of Defense/ Defense Advanced Research Projects Agency through grant MDA 972-97-1-003.

2 December 1999; accepted 7 February 2000

Efficient Activation of Aromatic C–H Bonds for Addition to C–C Multiple Bonds

Chengguo Jia, Dongguo Piao, Juzo Oyamada, Wenjun Lu, Tsugio Kitamura, Yuzo Fujiwara*

Efficient electrophilic metalation of aromatic C–H bonds leading to new C–C bond formation through regio- and stereoselective addition to alkynes and alkenes has been realized by a catalytic amount (0.02 to 5 mole percent) of palladium(II) or platinum(II) compounds in a mixed solvent containing trifluoroacetic acid at room temperature. Various arenes undergo unexpected selective trans hydroarylation to terminal or internal C≡C bonds inter- and intramolecularly with high efficiency (up to a turnover number of 4500 for palladium), especially for electron-rich arenes, giving thermodynamically unfavorable *cis*-alkenes, and the oxygen- and nitrogen-containing heterocycles. The simplicity, generality, and efficiency of this process should be very attractive to the possible industrial application for the functionalization of arenes.

Arenes such as benzenes, naphthalenes, phenols, and anilines are the large-quantity chemicals manufactured by chemical industries. Catalytically efficient activation of aromatic C–H bonds leading to useful organic reactions such as new C–C bond formation is of considerable interest for the chemical and pharmaceutical industries and remains a long-term challenge to chemists (*1*–*4*). It would provide simple, clean, and economic methods for making aryl-substituted compounds directly from simple arenes because no prefunctionalization, such as halogenation, is involved. The catalytic systems for such a purpose have been sought for many years, although there are many examples of stoichiometric reaction of aromatic C–H bonds with transition metal compounds (*1, 2*).

The few available catalytic systems based on transition metals (*4*–*12*) activate aromatic C–H bonds mainly through two routes. The first route is by chelation-assisted oxidative insertion of low-valent transition metal complexes, such as Ru(0) (*4, 5*) and Rh(I) (*6*) complexes, to aromatic C–H bonds in the hydroarylation of C–C multiple bonds. This insertion involves the coordination of a functional group in arenes to the metal complex, followed by the oxidative insertion of the metal to an ortho-aromatic C–H bond, resulting in the addition to unsaturated C–C bonds (*2*). These systems are apparently limited to functionalized arenes such as aromatic ketones at high temperature and give low stereoselectivity in the hydroarylation of alkynes. The second route involves electrophilic metalation of aromatic C–H bonds by Pd(II) complexes to give σ-aryl-Pd complexes in oxidative coupling of arenes with olefins in acetic acid (reaction 1 in Fig. 1). The σ-aryl-Pd complexes undergo cis aryl-palladation to C=C bonds followed by Pd-β-hydride elimination to give aryl alkenes (*9*–*12*). For this system, in situ regeneration of Pd(II) from Pd(0) is the crucial step for the catalytic cycle; the turnover number (TON) (the molar ratio of product formed to the catalyst) is still not high enough for possible industrial application. Therefore, it is still very desirable to find new, general, and efficient catalytic systems to activate the aromatic C–H bonds. Very few examples are available for the intramolecular version of this reaction type.

Department of Chemistry and Biochemistry, Graduate School of Engineering, Kyushu University, Hakozaki, Fukuoka, 812–8581, Japan.

*To whom correspondence should be addressed. E-mail: yfujitcf@mbox.nc.kyushu-u.ac.jp

We report the efficient metalation of aromatic C–H bonds at room temperature by in situ generated highly electrophilic Pd(II) and Pt(II) cationic species in trifluoroacetic acid (TFA), leading to regio- and stereoselective addition of simple arenes to C–C multiple bonds inter- and intramolecularly (reactions 2 through 4 in Fig. 1). In most cases, the addition to alkynes exclusively affords the thermodynamically unfavorable *cis*-aryl alkenes, unlike most of the arylmetalations of C≡C and C=C bonds that occur mainly in a cis fashion and yield trans products, especially in Pd-catalyzed reactions (*13, 14*). The intramolecular hydroarylation of C≡C bonds is very fast and regiospecific because the electrophilic metalation of aromatic C–H bonds by Pd(II) cationic species is assisted by ethynyl coordination, affording heterocycles in good to excellent yields. In fact, this intramolecular reaction combines the chelation assistance and electrophilic metalation.

The reaction of pentamethylbenzene with ethyl phenylpropiolate in a mixed solvent TFA/CH_2Cl_2 (4/1 by volume) at 25°C was used to screen catalysts among $Pd(OAc)_2$ (OAc, acetate), $Pd(PPh_3)_2(O_2CCF_3)_2$ (Ph, phenyl), $Pd(PPh_3)_4$, Pd/C, $PtCl_2$/2AgOAc, $RhCl_3$/3AgOAc, $IrCl_3$/3AgOAc, $RuCl_3$/3AgOAc, and $Ni(OAc)_2$. The highly electrophilic cationic species $[M(O_2CCF_3)_xL_y]^+$ (M, metal; L, ligand) are expected to be generated in situ through bonding weakly coordinating anions, $CF_3CO_2^-$, to transition metal ions by using TFA as a solvent (*15*–*18*). The cationic species should greatly enhance the metalation of aromatic C–H bonds and, at the same time, possibly activate C≡C and C=C bonds through the coordination to generate the acceptors of aryl nucleophiles. The reaction was carried out by simply mixing all of the reactants, a catalyst, and the solvent over an ice bath and then warming to room temperature (Table 1 and Fig. 2). The Pd(II) and Pt(II) catalysts were four times as active as other transition metals: Pd(II) > Pt(II) ≫ Rh(III) > Ru(III) > Ni(II), in accordance with the reactivity of these metal ions in electrophilic metalation of aromatic C–H bonds (*1*). The Pd(II) catalysts $Pd(OAc)_2$ and $Pd(PPh_3)_2(O_2CCF_3)_2$ are equally active; *cis*-ethyl 3-pentamethylphenyl cinnamate was obtained in 75% yield in 5 hours, and an almost